THz Frequency Selective Surface Filters for Earth Observation Remote Sensing Instruments

Dickie, R., Cahill, R., Fusco, V., Gamble, H., & Mitchell, N. (2011). THz Frequency Selective Surface Filters for Earth Observation Remote Sensing Instruments. IEEE Transactions on Terahertz Science and Technology, 1(2), 450-461. [5750080]. DOI: 10.1109/TTHZ.2011.2129470

Published in:
IEEE Transactions on Terahertz Science and Technology

THz Frequency Selective Surface Filters for Earth Observation Remote Sensing Instruments

Raymond Dickie, Robert Cahill, *Senior Member, IEEE*, Vincent Fusco, *Fellow, IEEE*, Harold S. Gamble, and Neil Mitchell, *Senior Member, IEEE*

***Abstract*—The purpose of this paper is to review recent developments in the design and fabrication of Frequency Selective Surfaces (FSS) which operate above 300 GHz. These structures act as free space electromagnetic filters and as such provide passive remote sensing instruments with multispectral capability by separating the scene radiation into separate frequency channels. Significant advances in computational electromagnetics, precision micromachining technology and metrology have been employed to create state of the art FSS which enable high sensitivity receivers to detect weak molecular emissions at THz wavelengths. This new class of quasi-optical filter exhibits an insertion loss <0.3 dB at 700 GHz and can be designed to operate independently of the polarization of the incident signals at oblique incidence. The paper concludes with a brief overview of two major technical advances which will greatly extend the potential applications of THz FSS.**

***Index Terms*—Frequency selective surfaces (FSS), liquid crystals, mesh filters, micromachined structures, polarization converter, quasi-optical technology, THz filters.**

I. Introduction

OVER the past decade major advances have been made in space borne THz instrument technology, primarily to address the need to study the processes driving the climate, and to monitor the changes and provide a health check on the environment in which we live [1]. This requires complex imaging of clouds [2] and spectroscopic characterization of carbon dioxide and other greenhouse gases in the Earth's atmosphere using remote sensing instruments which operate over wide bandwidths covering the thermal emission lines of the gases being observed [3]. To satisfy satellite payload constraints on cost, mass and energy consumption, passive Earth observation radiometers traditionally employ a single mechanically scanned aperture antenna to collect the radiation. Frequency selective surface (FSS) demultiplexing elements are a key enabling technology for these advanced instruments and are used in the quasi-optical receiver to spectrally separate the signals that are collected by the scanning antenna [3]. The key technology challenge is to ensure that the FSS exhibit very low signal band insertion loss and simultaneously meet the conflicting requirement for high isolation between adjacent frequency bands. This is required to minimize the overall noise performance of the instrument and thereby achieve high receiver sensitivity which is necessary to detect weak molecular emissions at THz wavelengths. In addition the FSS must also exhibit high performance at large incident angles to reduce the footprint of the feed train and moreover the structure should be sufficiently robust to withstand the launch forces of the space vehicle and operate without failure in the harsh thermal environment.

The purpose of this paper is to acquaint the reader with the principle application of this technology and to present an overview of a multidisciplinary research project at Queen's University Belfast (QUB) which has exploited state of the art developments in silicon microtechnology to create a new class of substrateless FSS that satisfies the electromagnetic requirements for remote sensing instruments that will enter service in the 21st century. These FSS will operate at 45° incidence and exhibit very high mechanical strength and suitable CTE properties. In addition to the use of new micromachining technology, innovative electromagnetic design strategies and measurement techniques have been employed to create quasi-optical filters which can separate either linear or simultaneously separate vertical and horizontal polarized components of naturally occurring thermal emissions with spectral efficiencies exceeding 93% at frequencies up to 700 GHz. The electromagnetic performance exhibited by this new class of FSS is presented for the MARSCHALS airborne limbsounder (294–380 GHz) [4], [5], European Space Agency (ESA) dual polarization FSS technology demonstrator (316.5–358.5 GHz) [6] and the Microwave Imager (MWI) instrument (113–670.7 GHz) which is currently being developed for the European Post EPS mission [2]. This paper concludes with a brief overview of two new innovative THz FSS structures which are currently being developed at QUB. One FSS variant provides conversion from linear to circular polarization whereas the other structure exhibits electronic shutter operation by exploiting the dielectric anisotropy property of nematic state liquid crystals.

II. FSS Design and Spectral Performance

A. Evolution of FSS Architecture

Radiometric remote sensing instruments in service before 2000 were generally designed to collect data using a single aperture antenna and drilled plate waveguide filters were deployed in the quasi-optical feed train to separate the signals and direct these to the spatial location of the individual channel mixer

Manuscript received January 28, 2011; revised March 04, 2011; accepted March 04, 2011. This work was supported in part by ESA under Contract 19854/06/NL/JA, EPSRC under Grant EP/E01707X1 and Grant EP/S13828/01, by EADS Astrium UK, CEOI (www.ceoi.ac.uk), and by the European Regional Development Fund under the European Sustainable Competitiveness Programme for Northern Ireland.

The authors are with The Institute of Electronics, Communications and Information Technology, The Queen's University of Belfast, Belfast BT3 9DT, Northern Ireland, U.K. (e-mail: r.cahill@ecit.qub.ac.uk).

Color versions of one or more of the figures in this paper are available online at http://ieeexplore.ieee.org.

Digital Object Identifier 10.1109/TTHZ.2011.2129470

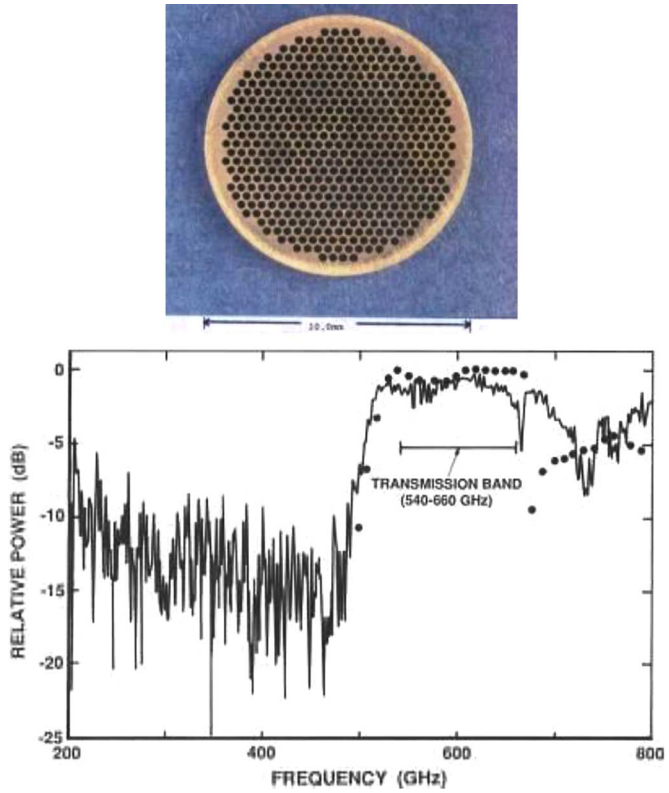

Fig. 1. 10 mm diameter 600 GHz waveguide FSS—TM 15° [8], [9].

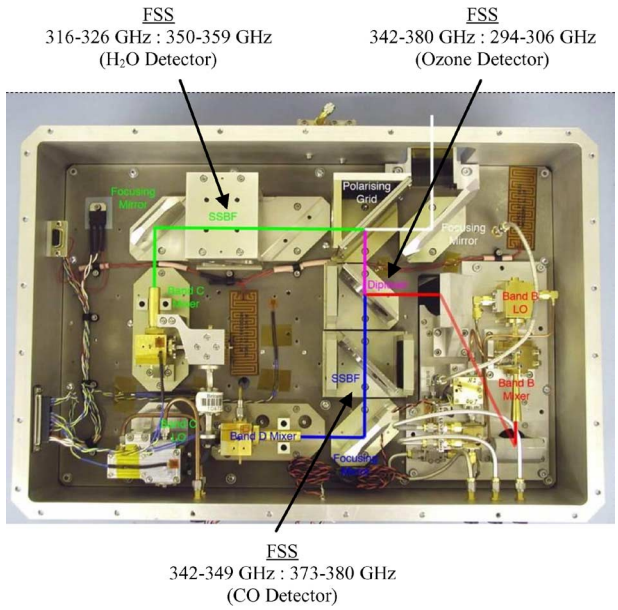

Fig. 2. MARSCHALS quasi-optical feed train—*courtesy of STFC*.

detectors. For example the 'Advanced Microwave Sounding Units (AMSU-B) which were launched on NOAA-15, 16, and 17 satellites between 1998–2002, used two waveguide array FSS to separate three signals bands centered at 89, 150, and 183 GHz [7]. The structures were fabricated using a computer controlled mill to precision drill an aluminum disk to the nominal dimensions of the two close packed arrays. Although this type of FSS is mechanically robust the spectral response is very sensitive to angle of incidence, the insertion loss can be high and the structures lacks design flexibility because the filter only provides high pass mode operation. Nevertheless until the beginning of the millennium this was the only space qualified method available to construct compact devices for spatially separating signals at millimeter wavelengths. To address the need to move to THz wavelengths in which there are resonances of ClO, BrO, HCl, and NO, an FSS demonstrator was designed to operate at 15° incidence and allow transmission of 540–660 GHz radiation and reject signals below 500 GHz. Fig. 1 depicts a photograph of the structure and the predicted and measured spectral response where it is shown that the transmission insertion loss is in the range 0.5–2.0 dB [8], [9].

Post AMSU-B a more versatile architecture consisting of printed FSS became available. These had the advantage that they could easily be designed to operate at large incident angles, in high pass, low pass and bandpass modes [10]. Furthermore conventional photolithographic techniques similar to those used in the semiconductor wafer industry were employed to print the periodic structures which generally consist of strongly shaped metal elements. The substrate choice for space science instruments is SiO_2 since this material is space qualified and the electrical design parameters are precisely known [11]. Structures of this type are employed in the Millimetre-wave Airborne Receiver for Spectroscopic CHaracterisation of Atmospheric Limb-Sounding (MARSCHALS) radiometer which is currently being developed by a European consortium led by Rutherford Appleton Laboratories in the U.K. [4]. The main objective of the instrument is to measure vertical profiles of ozone, water vapor, carbon dioxide and other gaseous components in the upper troposphere. Three printed FSS are deployed in the quasi-optical feed train, two function as image band rejection filters which separate the bands 316–326 GHz/350–359 GHz, 342–349 GHz/373–380 GHz, and the third FSS is used to provide demultiplexing of the channels 342–380 GHz/294–306 GHz. A photograph of the instrument and the location of the three filters are depicted in Fig. 2. The FSS were constructed from ring element arrays printed on opposite sides of quartz wafers of thickness in the range 100–130 μm. The structures allow transmission of radiation with a maximum insertion loss 1.0–1.5 dB in the TM 45° plane and for all three FSS the image/channel band rejection is better than 10 dB. The filter architecture and spectral performance are similar to a FSS which was designed to separate the signal band 297–304.5 GHz from the image band 275–282 GHz in the Advanced Microwave Atmospheric Sounder (AMAS) [12]. This instrument was developed by Rutherford Appleton Laboratories under contract to Dornier GmbH. An SEM and a plot comparing the measured and simulated spectral response are depicted in Fig. 3. The MARSCHALS and AMAS radiometers are designed to separate signal channels which are very closely spaced, with edge of band frequency ratios in the range 1.053:1–1.12:1. For this reason the structures require two periodic screens to achieve the fast transmission roll off which is required below resonance [9]. However the insertion loss of multilayer printed FSS is inversely proportional to the signal channel spacing [11] and therefore this can compromise the performance of the instrument. Moreover, another major practical consideration is

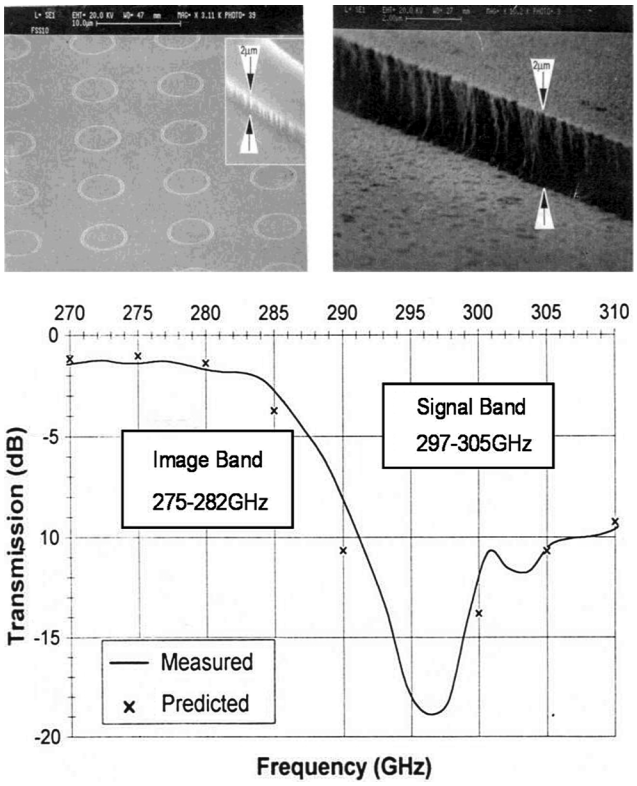

Fig. 3. Scanning electron micrograph (SEM) and spectral transmission of the AMAS FSS—TM 15° incidence [12].

the structural integrity of dielectric backed FSS. For example to achieve <1.5 dB insertion loss and 18 dB isolation between two channels centered at 501 and 550 GHz [8], a two-layer ring FSS was designed using a quartz wafer of thickness 70 μm. Although the specified electromagnetic performance was satisfied, the structure was too fragile for deployment in airborne and space science instruments, therefore, this observation suggests that the maximum operating frequency of high-Q printed FSS is far below 500 GHz.

B. Freestanding Mesh FSS

A new class of substrateless FSS has been developed to overcome the main drawbacks of printed structures, namely the higher than desirable insertion loss which is unavoidable because of the unavailability of alternative space qualified materials with a lower loss tangent at THz wavelengths, and the fragility of thin quartz wafers. In the 1960's an intensive study started into slot type periodic surfaces in an attempt to address the need to reduce the radar crossection of missile radomes. A patent [13] was granted to Professor Munk in 1978 for a two-layer slot FSS which exhibits a bandpass filter response with sharp skirts above and below resonance. This arrangement provided a narrow transmission window for the on board missile guidance radar however at out of band frequencies the FSS scatters the signals incident on the conical radome thereby reducing the radar crossection of the target. In 2001 [14] the deployment of substrateless slot FSS in radiometers operating at THz wavelengths was proposed as a solution to overcome the spectral and mechanical limitations of classical printed filters.

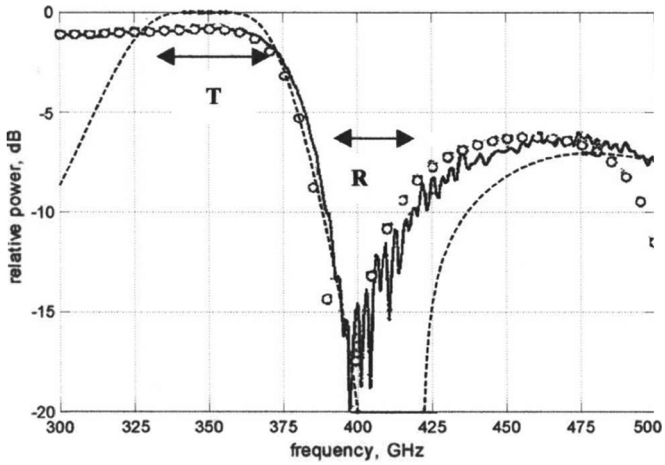

Fig. 4. Comparison between transmission response of 2 layer ring FSS with SiO_2 spacer and a 2 layer air spaced FSS—TM 45° incidence (*solid line and open circles measured and predicted* SiO_2 *backed FSS*) [14].

The efficiency enhancement was quantified by comparing the spectral transmission of a two layer freestanding FSS with a classical printed FSS in the frequency range 300–500 GHz. The simulated results depicted in Fig. 4 highlight the large increase in the signal transmission (1 dB) in the 350 GHz channel and the increase in the depth and bandwidth of the rejection band centered at 410 GHz.

Two or more self supporting screens each consisting of an array of slot elements is required to design and construct the FSS. The importance of removing all of the substrate material in the resonant elements is essential because as shown in [15] the insertion loss measured for dipole and dogbone slot FSS screens backed by high resistivity silicon is typically 1.6 dB at 300 GHz. The manufacturing route must be capable of creating high conductivity perforated metal structures that are substrateless, rigid and optically flat. In [16] two different fabrication technologies were employed to construct 300 GHz high-Q multilayer FSS. One manufacturing route used electroplating to create a low stress copper layer around patterned photoresist pillars with the same dimensions as the slot elements. The individual 30 mm diameter, 10 μm thick solid metal perforated screens were formed on the center portion of 2 inch quartz wafers by removing the pillars in an ultrasonic bath and chemically etching the back surface of the handle wafer. This approach employs several newly developed processing steps to improve on previously reported techniques for constructing an electrically thick dichroic plate which was designed to have a cut-off frequency of 950 GHz [17], and freestanding crossed dipole FSS operating in the range 585 GHz to 2.1 THz [18]. The second fabrication method employs an 8 μm thick layer of polymer which is etched to form the slot array and then totally encapsulated in 1 μm of aluminum. As in the previous case the structure is fabricated on a 2 inch quartz wafer which is etched away from one side to produce the 30 mm diameter FSS. Prior to this slot arrays had been printed on 3.8 μm thick polyester films and these exhibited an insertion loss of 1.9 dB at 2.2 THz [19]. From these reported developments it became clear that the fabrication technologies were suitable for constructing thin periodic screens consisting of simple dipole slots, however because of cantilever droop, they

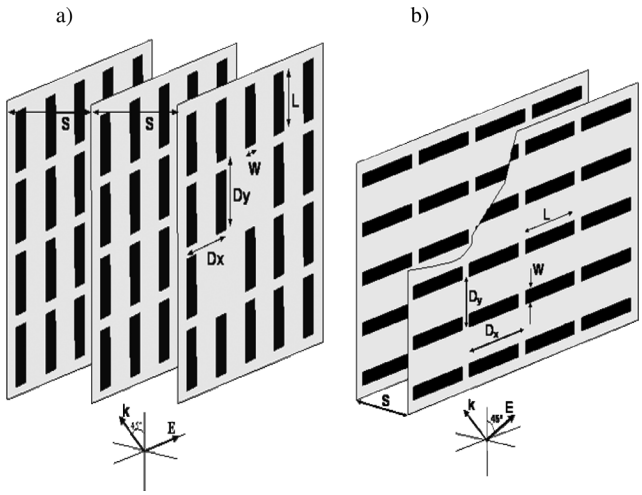

Fig. 5. Free standing resonant slot FSS filters [5] (a) Three-layer TE FSS $L = 460\ \mu$m, $W = 15\ \mu$m, $D_x = 490\ \mu$m, $D_y = 500\ \mu$m, $S = 357.5\ \mu$m (b) Two-layer TM FSS $L = 470\ \mu$m, $W = 20\ \mu$m, $D_x = 540\ \mu$m, $D_y = 452\ \mu$m, $S = 143\ \mu$m.

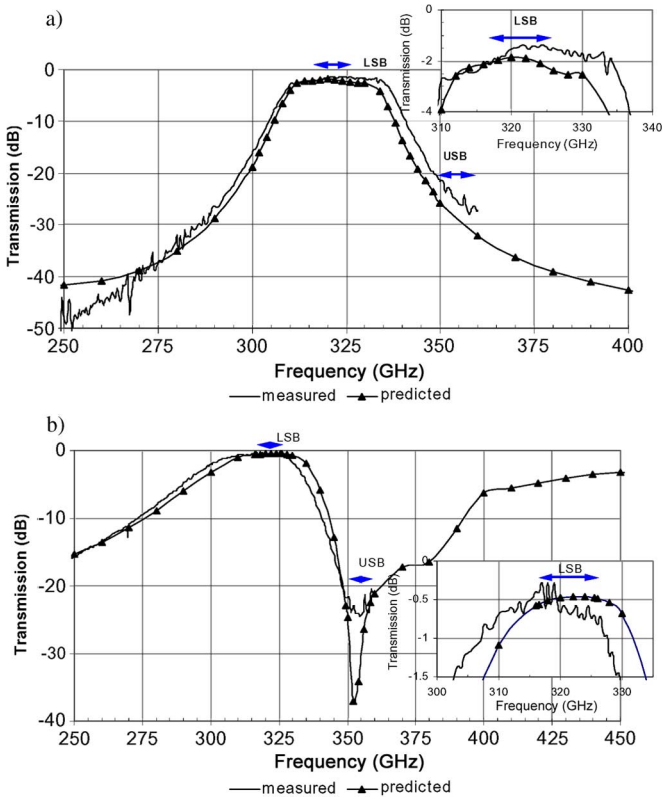

Fig. 6. Computed and measured frequency response of freestanding FSS at 45° incidence. (a) Three-layer TE. (b) Two-layer TM [5].

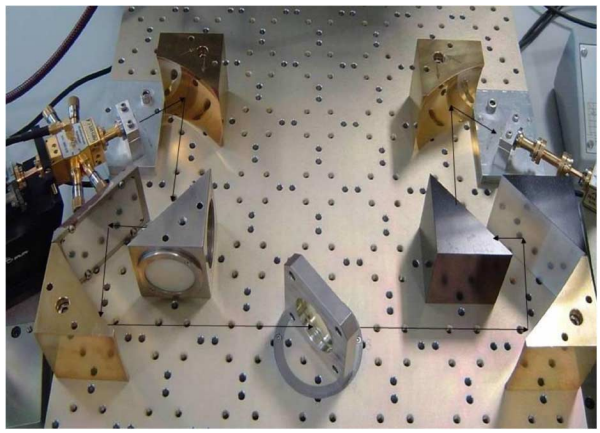

Fig. 7. Quasi-optical transmission test setup.

were not suitable to construct arrays of more highly shaped elements, such as those shown in Figs. 13 and 16. Building on this observation, we developed advanced silicon micromachining processes to manufacture ultra low loss multilayer mesh filters for space science instruments operating at THz wavelengths [6]. These are shown to be robust and give a better spectral performance than drilled plate and printed periodic arrays. The improved transmission efficiency afforded by the freestanding FSS architecture was demonstrated experimentally by designing a structure using the specified frequency separation plan of the Band C single sideband filter of the MARSCHALS radiometer. The spectral response [5] was then compared to a printed FSS previously supplied by QUB and deployed in the instrument which has since undergone flight trials. The latter filter yielded approximately 1.5 dB insertion loss in the signal (lower side) band (LSB: 316.5–325.5 GHz) and 20 dB isolation of the image (upper side) band (USB: 349.5–358.5 GHz) when operated at 45° incidence in the TM plane. Given that the instrument is required to detect either TE or TM polarized signals, freestanding FSS designs were optimized to give the lowest signal transmission loss and simultaneously exhibit a minimum channel isolation of 20 dB for both orientations of the incident electric field. The geometry of the two arrangements and the dimensions used to define the computational unit cell within HFSS [20] are depicted in Fig. 5. The optimum performance in the TE plane is obtained with three perforated screens, however for TM incidence a simpler structure consisting of just two periodic arrays was designed. Computed transmission coefficients between 250–400 GHz are plotted in Fig. 6. These show that the insertion loss of the TM polarized FSS at resonance (322 GHz) is approximately 1.0 dB lower than the printed FSS. For a perfect electrical conductor (PEC) the computed transmission at resonance is almost 100% therefore this result suggests that the efficiency factor is limited by Ohmic loss and not by reflections from the screens. The insertion loss of the three-layer TE polarized FSS is in the range 1.8–2.2 dB, however when modeled as a PEC this reduces to 0.5 dB. The transmission response of the two FSS was measured using an AB vector network analyzer [21] in conjunction with a quasi-optical test bench. The feed train employs two wideband corrugated feed horns at the waveguide ports of the source and detector and ellipsoidal mirrors which focus the Gaussian beam to produce a beam waist radius of approximately 4 mm at the position of the FSS in the feed train. The edge illumination on the 30 mm diameter filter orientated at 45° is lower than 35 dB, and so beam truncation effects can be neglected [22]. The S_{21} measurements were performed by ratioing the spectra with and without the FSS in the sample holder, QO bench and holder as shown in Fig. 7. Excellent agreement

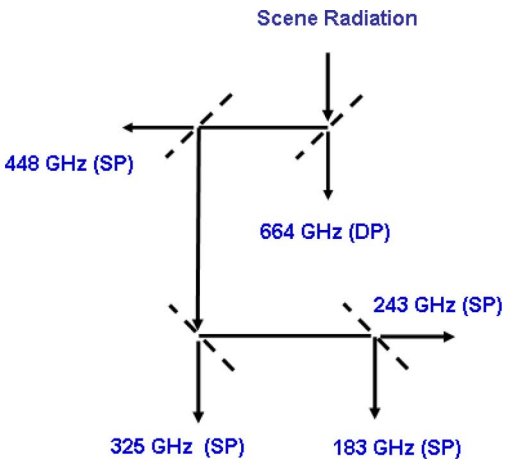

Fig. 8. MWI radiometer quasi-optical feed train layout. (DP) is dual polarization; (SP) is single linear polarization.

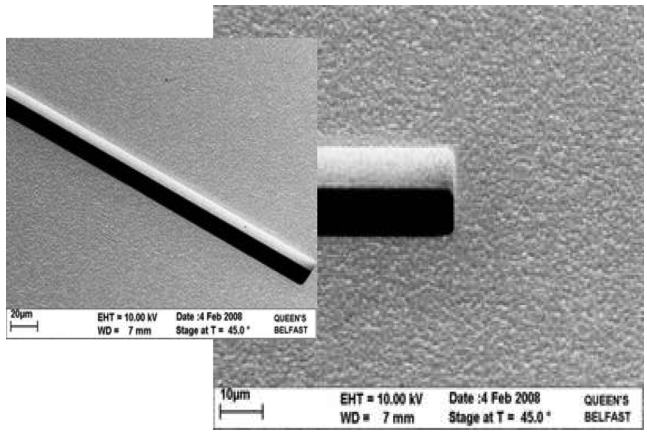

Fig. 9. SEM images of 448 GHz MWI FSS [23].

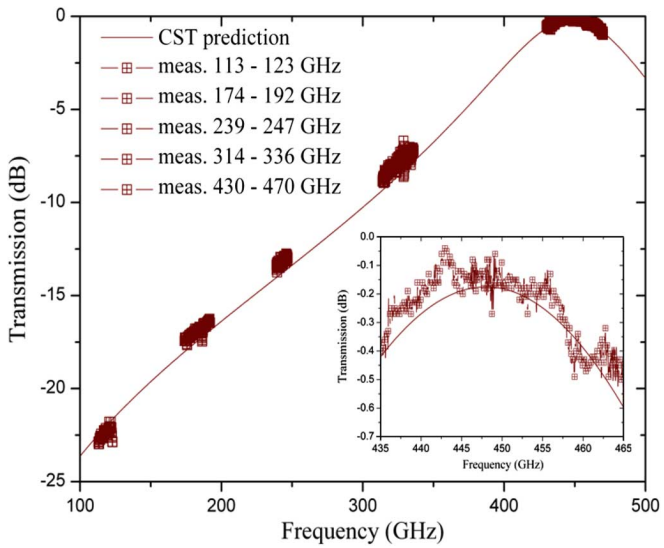

Fig. 10. CST predictions and measured transmission coefficients of the MWI 448 GHz FSS in discrete frequency channels—TM 45° incidence.

between the simulated and measured spectral responses is observed in Fig. 6. The two-layer FSS shown in Fig. 5(b) was retrofitted to the MARSCHALS radiometer and subsequently the remaining two printed quartz FSS were also replaced by high performance freestanding structures. Measured system level results obtained from recently completed airborne flight trails confirmed the expected improvement in the instrument sensitivity.

The Microwave Imager Instrument (MWI) [2] is an advanced passive radiometer that is currently being developed by the European Space Agency to provide complex imaging of clouds. Retrieved data obtained from the space science instrument will be employed in numerical prediction models to improve the accuracy of medium and long term weather forecasting [23]. This mission is part of the Post EPS mission to replace the MetOp satellites in the 2018–2020 time frame. FSS are required to provide spatial separation of the scene radiation into five narrow channels centered at 664 GHz (2%), 448 GHz (3.6%), 325 GHz (6.8%), 243 GHz (3%), and 183 GHz (10%). All but the 664 GHz FSS are required to transmit (and reflect) linearly polarized signals, with the electric field vector orientated vertically or horizontally. One proposed layout of the quasi-optical feed train is depicted in Fig. 8. Spatial separation of the 448 GHz channel from the three lower frequency bands requires an FSS which exhibits a maximum insertion loss of 0.5 dB in the transmission band and <1 dB loss in the four reflection channels. The optimum design consists of a single screen FSS perforated with 326 μm long dipole slots as shown by the SEM images in Fig. 9, and arranged in a rectangular lattice. The computed insertion loss of the FSS is 0.2 dB at the passband centre (448 GHz) and 0.3 dB at the upper and lower passband edges. The numerical simulations were performed using the frequency domain solver of CST MICROWAVE STUDIO [24]. The screen thickness, 12.5 μm, and the bulk conductivity value of silver, 6.17×10^7 S/m, were included in the computer model. At the upper edge of the three lower frequency channels the computed reflection loss is 0.85 dB (336 GHz), 0.22 dB (247 GHz), and 0.11 dB (192 GHz). In Fig. 10 the experimental spectral transmission coefficients are shown to be in very close agreement with the numerical results. Similar agreement was observed for the reflection responses (not shown for brevity) and the maximum measured loss was found to be 0.76 dB (336 GHz) which exceeds the performance specified for the MWI optical filter elements.

C. Dual Polarization Freestanding Mesh FSS

Passive remote sensing of the atmosphere from space in the frequency range 100–500 GHz is currently performed using linear polarized molecular emission spectroscopy. Therefore to address this technology need, research over the past decade has focused on creating FSS structures which separate signals with electric vectors that are either orientated parallel (TM) or perpendicular (TE) to the plane of incidence. In 2007 a major extension to this work was initiated to provide a technical solution to facilitate the detection and analysis of dual polarized radiation. This additional capability will be incorporated in future space science missions that are planned by ESA. The data retrieved will provide information on the size and shape of water ice particles in cirrus clouds and these observations will ultimately be used to quantify their effect on the Earth's radiation budget.

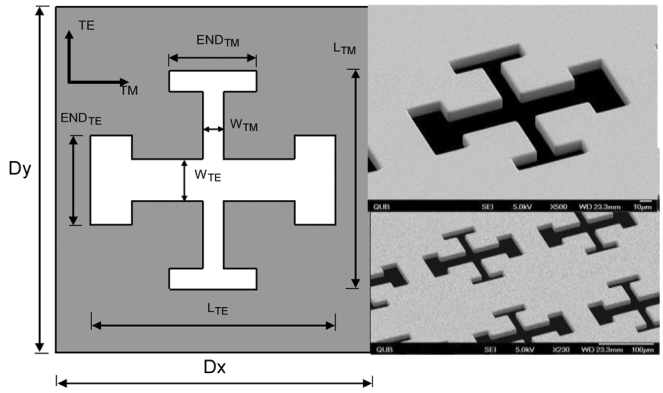

Fig. 11. Geometry and dimensions (μm) of unit cell, and scanning electron micrographs of MWI 664 GHz FSS [23] $L_{\mathrm{TM}} = 158$, $L_{\mathrm{TE}} = 179$, $W_{\mathrm{TM}} = 15$, $W_{\mathrm{TE}} = 30$, $\mathrm{END}_{\mathrm{TM}} = 64$, $\mathrm{END}_{\mathrm{TE}} = 65$, $Dx = 230$, $Dy = 250$.

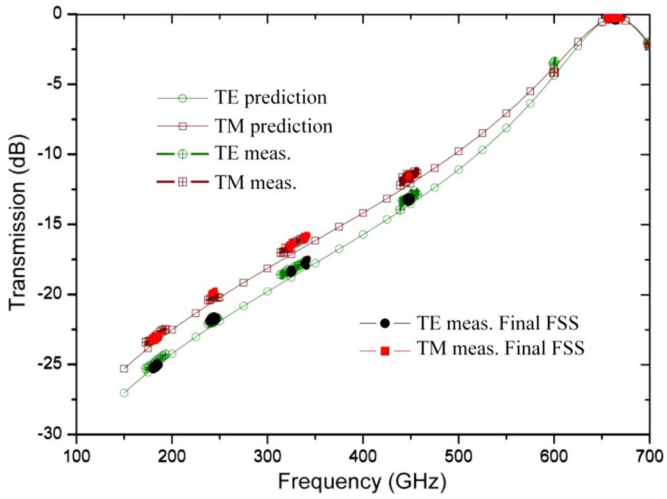

Fig. 12. Computed and measured spectral responses of the MWI 664 GHz dual polarization FSS [23]—the plot also shows the measured response of a second technology demonstrator 'Final FSS'.

For these instruments innovative freestanding FSS filters are required to simultaneously operate in dual polarized mode when the filter is orientated at 45° to the incident beam.

The first European Earth observation radiometer which will require a polarization independent THz FSS is the MWI instrument. Fig. 8 shows that the first FSS is required to separate the 664 GHz channel from the four lower frequency bands (63% bandwidth) when the filter operates in *both* the TE and TM planes and is orientated at oblique incidence in the radiometer.

The specified maximum signal loss in the transmission and reflection bands is 0.5 dB and for this application the frequency separation ratio of the FSS is 1.44:1 (657.3/456.7 GHz), therefore a single freestanding screen can satisfy the requirements. The geometry and dimensions of a unit cell of the Jerusalem Cross FSS is depicted in Fig. 11. Coincident spectral responses were obtained by adjusting the individual lengths of the vertical and horizontal main arms and increasing the physical width of the latter to remove passband narrowing which is observed when the structure is excited by a TE polarized wave at 45° incidence. Moreover the capacitive loading introduced by the end caps of the Jerusalem Cross elements reduces the area occupied by the slot in each unit cell and this increases the structural integrity of the filter. The predicted and measured results are depicted in Fig. 12 where it is shown that the maximum loss in the transmission and reflection band is below 0.5 dB in both planes of polarization. The numerical simulations, which included the finite conductivity of the metal, were performed using the frequency domain solver of CST.

The design of a polarization independent FSS is significantly more complicated when the transmission and reflection bands are very closely spaced. Suitable topologies that can be employed to create a FSS which separates the Band C signal (316.5–325.5 GHz) and image (349.5–358.5 GHz) channels of the MARSCHALS radiometer have recently been studied. Fig. 13 shows a periodic array of nested short circuited annular slots which can be designed to provide spatial demultiplexing of the two channels (frequency separation ratio of 1.07:1). At the specified centre operating frequency (321 GHz) the length of the inner slot is $\approx \lambda/2$ and the outer slot length is $\approx \lambda$. Therefore when these are excited by TM and TE polarized waves, respectively, the structure resonates at the same frequency and

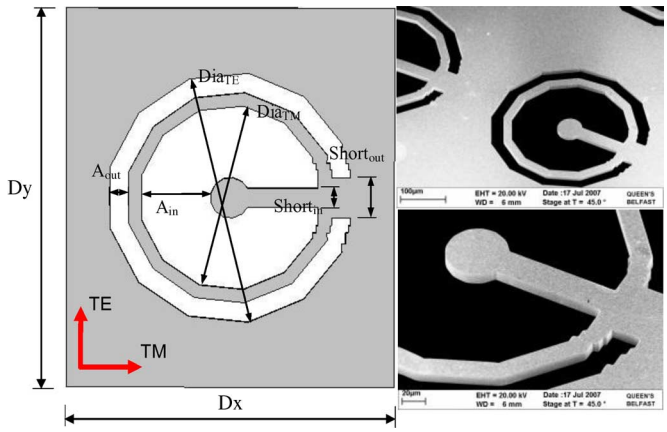

Fig. 13. Geometry and SEM of prototype dual polarized annular slot FSS [25] $Dx = 475\ \mu$m, $Dy = 540\ \mu$m, $A_{\mathrm{in}} = 102\ \mu$m, $A_{\mathrm{out}} = 27\ \mu$m, $\mathrm{Short}_{\mathrm{in}} = 27\ \mu$m, $\mathrm{Short}_{\mathrm{out}} = 57\ \mu$m, $\mathrm{Dia}_{\mathrm{TM}} = 263\ \mu$m, $\mathrm{Dia}_{\mathrm{TE}} = 357\ \mu$m, $\mathrm{Depth} = 12.5\ \mu$m.

the orthogonally orientated signals transmit through the FSS. Optimization of the design was made by increasing the width of the inner slot to reduce the spectral roll-off rate above the passband in the TM plane and by employing two single screens separated by a distance 475 μm. One of the perforated screens was rotated by 180° to make full use of the interlayer coupling. The simulated copolar and cross-polar spectral responses are plotted in Fig. 14, where it is shown that the lower sideband and upper sideband spectral responses in the orthogonal polarization planes are coincident [25]. The numerical results were obtained from CST using a screen thickness of 12.5 μm and the bulk resistivity value of copper, $1.72 \times 10^{-8}\ \Omega \cdot$ m. These are in close agreement with the experimental results which show that the maximum passband loss is <0.9 dB, the crosspolar levels are >21 dB and the minimum image band rejection is 20 dB. Although dual polarization operation is demonstrated using the nested annular slot architecture, the electromagnetic performance falls short of the most demanding specifications imposed on FSS structures which are to be deployed in the

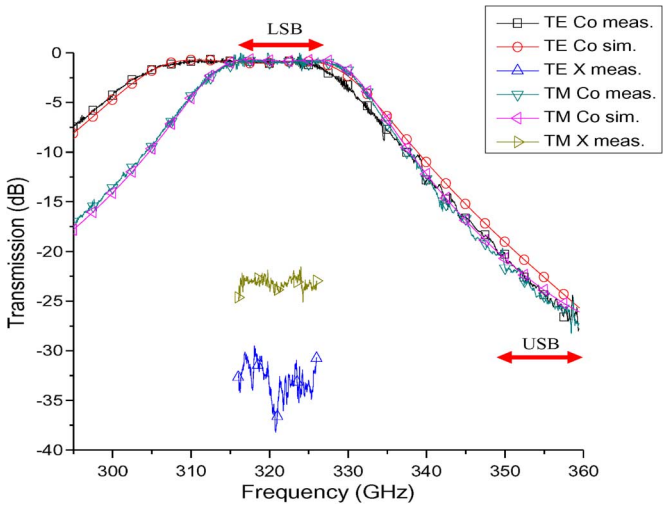

Fig. 14. Predicted copolar and measured copolar and cross-polar spectral response of two-layer annular slot FSS at 45° incidence in TE and TM plane [25].

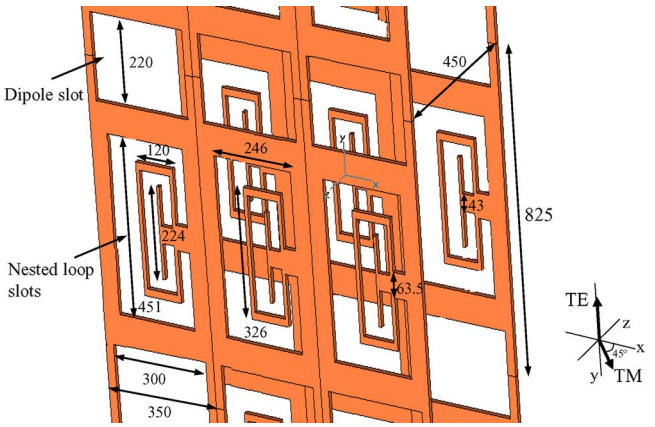

Fig. 15. Geometry and dimensions (μm) of the nested two-layer dual polarization FSS [6].

next generation passive radiometers. To achieve the desired receiver sensitivity the filter should ideally exhibit a maximum loss of 0.5 dB and simultaneously provide 30 dB channel isolation. Strategies for improving the spectral performance of the FSS plotted in Fig. 14 were investigated using detailed parametric studies. In common with the prototype FSS previously described, the design specification was also based on the MARSCHALS Band C single sideband filter. CST predictions were employed to show that a significant reduction in the insertion loss and higher channel isolation are obtained from a more advanced periodic array design. The unit cell of the two layer arrangement depicted in Fig. 15 consists of two nested short circuited rectangular loop slots and a rectangular dipole slot. Reference [6] describes the systematic design approach which was employed to achieve the desired filter performance. The electric field distribution at resonance (321 GHz) in the TM plane (inner slot) and the TE plane (outer slot) and a scanning electron micrograph image of three unit cells of the assembled and bonded two layer FSS are depicted in Fig. 16.

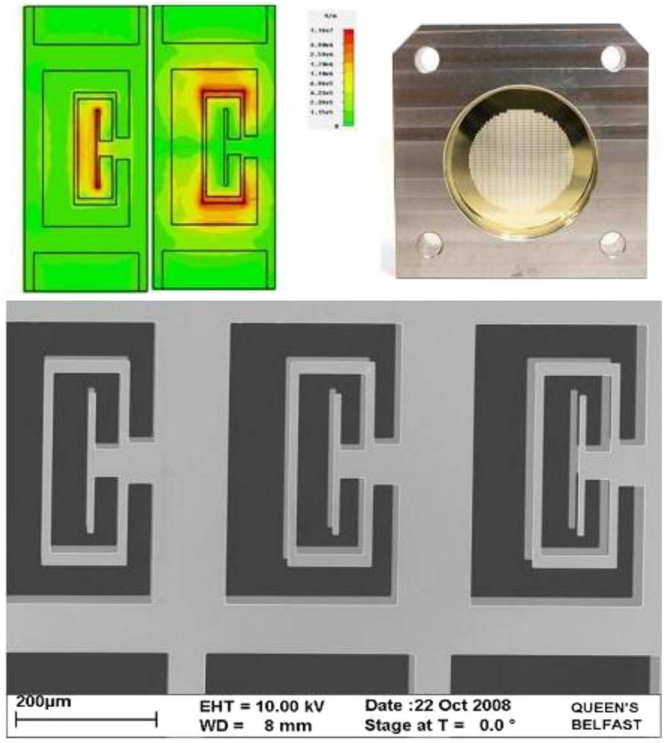

Fig. 16. Computed electric field distribution, SEM and photograph of the two-layer dual polar FSS mounted in an invar holder [6].

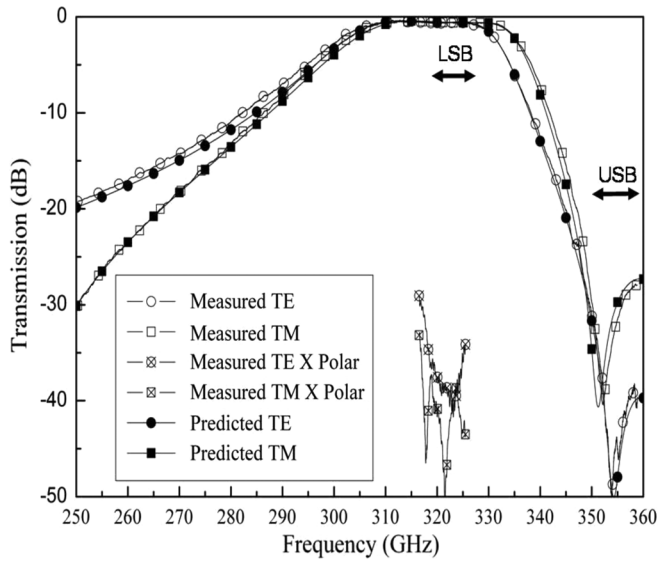

Fig. 17. Measured and computed spectral response of polarization independent FSS [6].

An additional resonance is generated at 450 GHz by the horizontally orientated linear slot. This design feature removes the undesirable effect of the weaker transmission roll-off which is observed above the passband in the TE plane thereby creating coincident reflection channels. The computed transmission coefficients using the bulk conductivity value of silver 6.17×10^7 S/m and the experimental results plotted in Fig. 17 show that a significant performance improvement is obtained. The structure exhibits a maximum insertion loss of 0.6 dB (316.5–325.5 GHz), >30 dB rejection (349.5–358.5 GHz) and

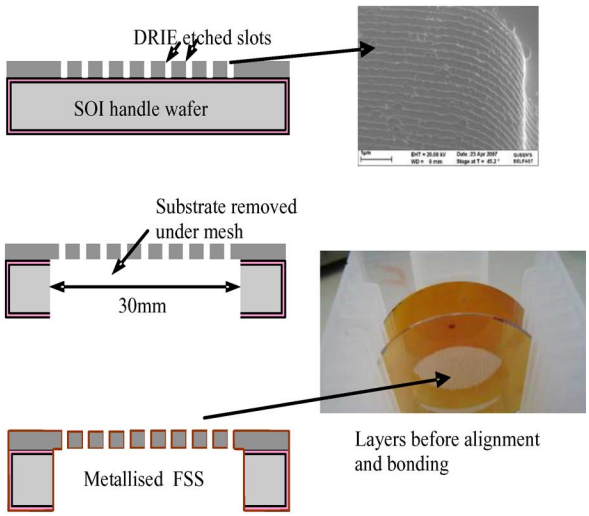

Fig. 18. Key processing steps used to construct one single FSS layer.

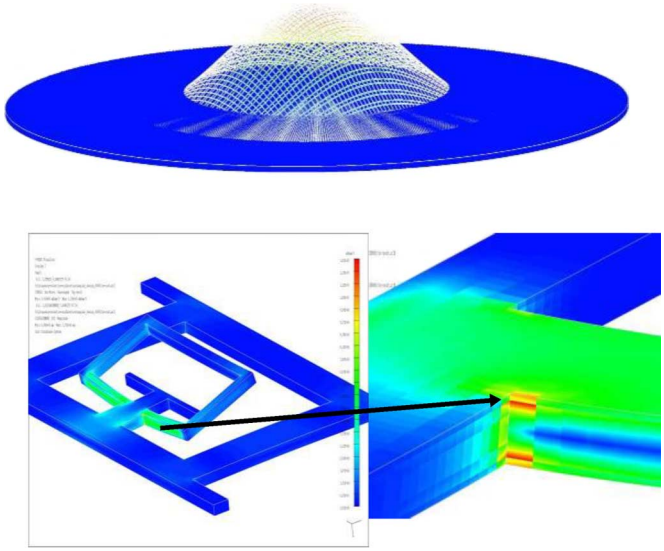

Fig. 19. FEM structural analysis showing the natural frequency and stress concentrations of the FSS [6].

cross-polar levels below -25 dB simultaneously for TE and TM polarizations at 45° incidence.

III. Fabrication and Space Qualification

The preferred manufacturing method is to form the individual perforated screens by high conductivity coatings on silicon wafers. Single crystal silicon was chosen as the base material of the structure because it has very high theoretical yield strength, typically 7000 MPa, and therefore provides a very rigid core with desirable structural properties. The FSS were constructed from 100 mm diameter silicon-on-insulator (SOI) material which consists of a handle silicon wafer (typically 400 μm thick) with a 3 μm buried oxide insulating layer on top of which is a 10 μm silicon surface. The SOI wafers are coated with photo resist and patterned to form a mask for the deep reactive ion etching (DRIE) of the 10 μm silicon layer which was etched at a rate of 3.5 $\mu\mathrm{m/minute}$. DRIE was used to remove the exposed silicon under the array and the release rings to create a 50 mm diameter freestanding structure containing the 30 mm diameter perforated FSS and a 10 mm wide silicon annulus with the same thickness as the handle wafer. The FSS was then sputter coated with a titanium adhesion layer followed by a 0.25μm thick copper seed layer. The construction was completed by growing a 1 μm thick electrodeposited silver coating on the seed layer and applying a 25 nm thick layer of gold to prevent oxidation. Fig. 18 summarizes the main processes steps for the single screen. When another layer was added separation was controlled by placing epoxy binder containing precisely dimensioned glass spheres around the screen annulus. The measured dimensional tolerances of the slot elements was found to be within ± 2 μm and the separation distance was within ± 5 μm of the nominal design value for the multilayer arrangements. A more detailed description of the fabrication and plating processes which were developed to construct the freestanding FSS arrays is given in [6].

The construction technique was selected to satisfy the structural and thermal demands of the space environment. This approach exploits the high mechanical strength and rigidity of silicon. Detailed mechanical analysis was carried out by EADS Astrium UK Ltd to quantify the dynamic behavior and peak stress levels of the structure, as shown in Fig. 19. The predicted natural frequency obtained from a finite element model of the 30 mm diameter structure is 148 Hz and therefore meets the minimum requirement with 48% margin. Fig. 19 also shows a single unit cell containing 50 000 mesh elements. This was used to model the stress contours during random vibration and the stress concentrations, which are shown above. The highest stress levels predicted in the silicon was 487 MPa which is more than ten times lower than the allowable yield (7000 MPa). Random and sine vibration testing in three axes was performed to space qualification levels at the EADS Astrium Portsmouth environmental test facility. In addition thermal cycling was used to demonstrate that the FSS can survive in—orbit temperatures. Five cycles between -20 °C and $+60$ °C with a dwell time of 1 hour was used to test the filter. Visual inspection before and after testing confirmed the robustness of the FSS and pre and post test spectral measurements showed no degradation in the spectral performance of the filter.

IV. Future Developments

A. FSS Polarization Convertor

A new concept for converting an incident linear polarized (LP) wave into circular polarization (CP) upon transmission through a split slot ring FSS has recently been demonstrated at 320 GHz. The unit cell geometry depicted in Fig. 20 consists of a nested arrangement of two annular slots suitably orientated [26] so that an incident slant 45° LP signal when resolved into equal components, aligned along the vertical and horizontal directions, exits the FSS with outputs that are equal in amplitude and have a phase difference of 90°. The length of the outer slot is slightly larger than one wavelength at the operating frequency of the polarizer thus the impedance presented by the FSS to the TE wave component at 320 GHz is inductive.

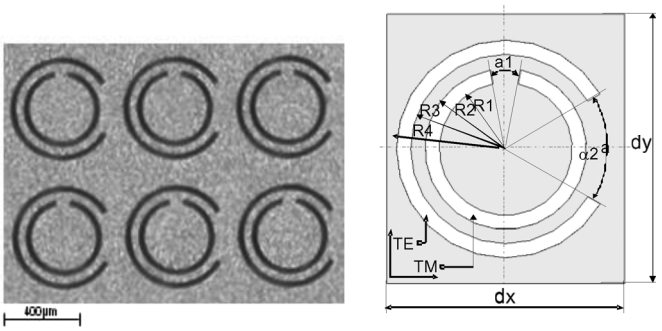

Fig. 20. SEM and geometry of single layer ring slot polarization converter design: $dx = 475\ \mu$m, $dy = 540\ \mu$m, $R1 = 133.6\ \mu$m, $R2 = 157.9\ \mu$m, $R3 = 189.5\ \mu$m, $R4 = 213.5\ \mu$m, $\alpha 1 = 16.8°$, $\alpha 2 = 53.6°$ [26].

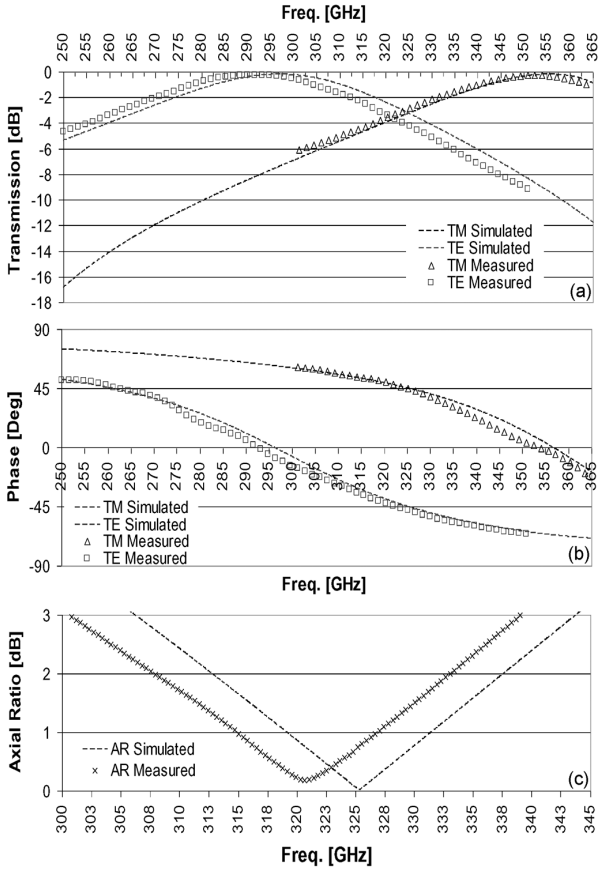

Fig. 21. Simulated and measured results: (a) amplitude; (b) phase; and (c) AR of transmitted CP signal [26].

Conversely for the TM signal the smaller inner slots create a capacitive reactance and thus the two criteria which are required to launch a CP wave [27] are satisfied by the single layer FSS. The screen dimensions shown in Fig. 20 were obtained from the frequency domain solver of CST using the conductivity of copper and the device was micromachined using the process steps outlined in Section III. The 30 mm diameter, 10 μm thick silicon reinforced metal structure contains 2700 resonator cells. Close agreement between the measured and predicted transmission, phase and axial ratio [27] is shown in Fig. 21. At 320.8 GHz, the axial ratio minimum, the measured phase difference is 88°

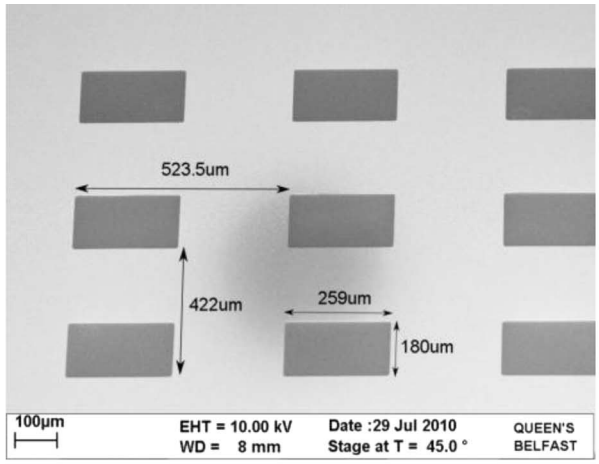

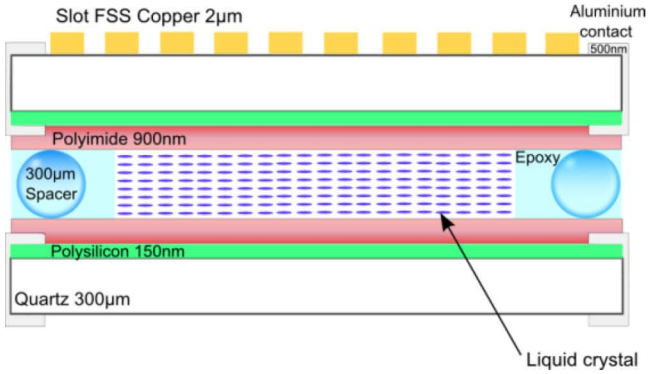

Fig. 22. Unit Cell geometry of the reconfigurable FSS device with dimensions; periodicity $dx = 422$ and $dy = 522$, slot width $w = 184$, slot length $l = 262$, quartz thickness $q = 300$, liquid crystal thickness $\mathrm{lc} = 300\ (\mu\mathrm{m})$ [29].

and the insertion loss is −3.38 dB. Previously the authors reported that a single layer polarization converter designed to operate at X-band yielded a similar loss, however computed and measured results also showed that this can be reduced to <0.5 dB by designing a double screen FSS [28].

B. Electronically Tunable FSS

A new class of adaptive FSS is currently being developed which allows a small voltage to switch 'on' and 'off' an incident signal thus producing an electronically controllable shutter [29]. The tunable bandpass filter response is obtained by exploiting the dielectric anisotropy property of a thin layer of nematic state liquid crystal (LC) molecules which is sandwiched between two electrodes as shown in Fig. 22. A technology demonstrator has been constructed using a 30 mm diameter printed FSS which consists of an array of 259 μm long rectangular slots. The periodic structure is formed on a 300 μm thick quartz wafer with a boron diffused polysilicon biasing layer formed on the bottom surface of the wafer. Another 300 μm quartz wafer is used to provide a second biasing layer and to encapsulate the liquid crystals. In the unbiased state $(\varepsilon_{//})$ the director of the liquid crystal molecules are orientated parallel to the surface of the quartz wafer due to the static action of a polyimide coating on the bias layer. To reconfigure the molecules a voltage is applied across the biasing layers producing a torque which rotates the

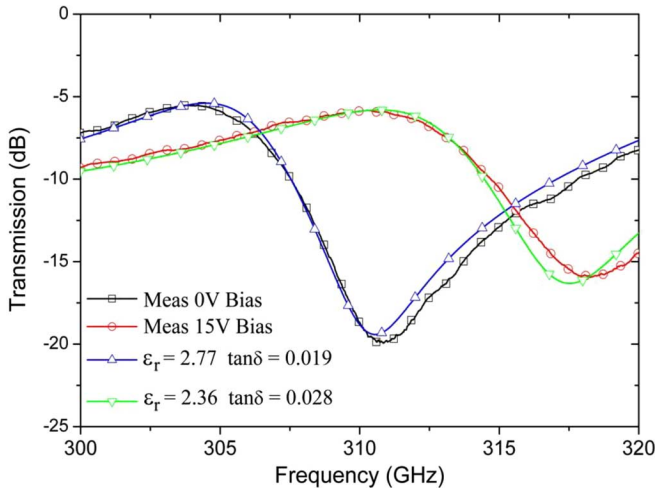

Fig. 23. Measured and predicted spectral response of experimental electronically reconfigurable liquid crystal based FSS [29].

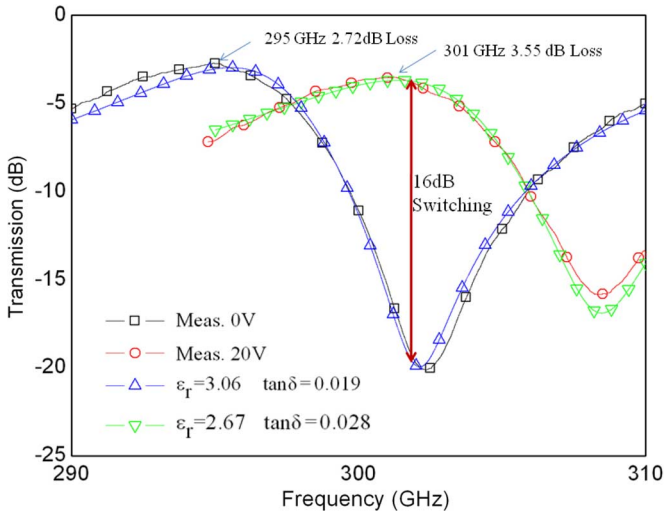

Fig. 24. Simulated and measured spectral response of optimized prototype electronically reconfigurable FSS based on BL037 liquid crystals.

molecules perpendicular to surfaces. This changes the permittivity value from $\varepsilon_{//}$ to $\varepsilon_{\perp}$. Once the voltage is switched off the molecules return to their parallel state due to the action of the polyimide alignment layer. The dielectric constant of the LC layer varies between these two states and the tunability is defined as

$$\Delta\varepsilon_{\text{eff}} = \varepsilon_{//} - \varepsilon_{\perp}.$$

The inherent dielectric anisotropy of the liquid crystals can therefore be exploited in this arrangement to shift the resonant frequency of the bandpass FSS thus creating a structure which can both block and be transparent to THz signals on demand. The experimental device was designed to reconfigure its passband in the frequency range of 290–310 GHz when oriented at 45° in TE plane. A 300 μm thick layer of Merck BL037 liquid crystals was sandwiched between the quartz wafers and this was modeled in CST using $2.8(\varepsilon_{\perp})\tan\delta = 0.01$ and $3.2(\varepsilon_{//})\tan\delta = 0.02$. These permittivity and loss tangent values are given in the literature at 130 GHz [30], however, as shown in Fig. 23, the experimental spectral response is better matched at THz wavelengths using $2.36(\varepsilon_{\perp})\tan\delta = 0.028$ and $2.77(\varepsilon_{//})\tan\delta = 0.019$ in the numerical model. The measured data was obtained with bias voltages of 0 and 15 V. This first technology demonstrator therefore confirms the design methodology and provides accurate characterization of the electrical properties of the liquid crystals in the frequency range 300–320 GHz. The spectral response of the electronically tunable FSS has been optimized using these values.

For operation at 45° incidence in the TE plane the slot length is increased to 272 μm, the periodicity decreased to 512 μm and in the numerical model a 350 μm thick LC layer was inserted in the cavity between the two quartz wafers. The periodic array was modeled using the conductivity of copper. Fig. 24 depicts the measured transmission response of the FSS in the unbiased state and with an applied 20 V peak to peak triangular waveform at 20 KHz. The measured filter bandpass centre resonant frequency is 295 GHz in the unbiased state and the insertion loss is about 2.7 dB. When the FSS is energized by a control voltage the frequency shifts upwards to 301 GHz and the loss increases to 3.5 dB. This produces a dynamic switching range of 16 dB at the upper resonance. In addition to demonstrating electronic shutter operation at 301 GHz it is noted that the FSS also provides electronic tuning of the passband peak over a 2% bandwidth. Excellent agreement with predicted results is obtained using permittivity values of 3.06 (0 V) and 2.67 (20 V) in the numerical model. It is noted that these are 10% larger than the measured design values for BL037 which were obtained from the results plotted in Fig. 23. BL037 is a commercially available liquid crystal material which has been engineered for optical applications, therefore, a significant improvement could be obtained by synthesizing a mixture which yields lower loss at THz wavelengths. The best possible performance was predicted by setting the loss tangent of the tunable layer to zero in CST. The computed spectral performance shows that with this arrangement the insertion loss of the electronically reconfigurable FSS is less than 0.9 dB and the dynamic switching range is greater than 35 dB.

V. Conclusion

In this review paper, the authors have briefly described many of the innovative design techniques and manufacturing processes that have led to the creation of state of the art FSS filters operating at THz wavelengths. Over the past 20 years the technology has mainly been driven by the need to satisfy the stringent electrical and mechanical performance specifications for separating signals in advanced Earth observation instruments. The manufacturing process developed at QUB is wholly compatible with the structural and thermal requirements for space hardware. Moreover, the substrateless FSS have very little impact on the receiver sensitivity and their use permits the deployment of a single reflector antenna to collect energy over a wide frequency band thus significantly reducing energy consumption, cost and the size and mass of the payload. New and innovative design strategies for converting from linear to circular polarization and for dynamically switching signals incident on the FSS have been demonstrated over the past

three years. These devices exploit the same computational analysis techniques and manufacturing processes that have been developed to produce space qualified demultiplexing filters. The additional functionality afforded by these FSS could find applications in imaging devices and other emerging THz technologies.

ACKNOWLEDGMENT

The studies reported in this paper were carried out at the Queen's University Belfast. The authors would like to acknowledge the contribution to this work which was made by Dr. P. de Maagt (ESA); Dr. N. Grant, Ms. Y. Munro, Prof. M. Johnson, and P. Howard (EADS Astrium); and Dr. P. Huggard, Dr. M. Henry, and B. Moyna (RAL).

REFERENCES

[1] C. Mangenot, "Space antennas: ESA's perspectives on future needs and technologies," presented at the 13th Int. Symp. on Antennas, Nice, France, 2004.

[2] V. Kangas, C. Lin, and M. Betto, "Microwave instrument requirements and technology needs for the post-EPS mission," in *Proc 31st ESTEC Antenna Workshop on Millimetre and Sub-Millimetre Waves—From Technologies to Systems*, May 2009, pp. 501–506.

[3] R. J. Martin and D. H. Martin, "Quasi-optical antennas for radiometric remote sensing," *Electron. Commun. Eng. J.*, vol. 8, pp. 37–48, Feb. 1996.

[4] M. Oldfield, B. Moyna, E. Allouis, R. Brunt, U. Cortesi, B. Ellison, J. Ellison, J. Eskell, T. Forward, T. Jones, D. Lamarre, J. Langen, P. de Maagt, D. Matheson, I. Morgan, J. Reburn, and R. Siddan, "MARSCHALS: Development of an airborne millimetre-wave limb sounder," in *Proc. SPIE 8th Int. Symp. on Remote Sensing*, Sept. 2001, vol. 4540, pp. 221–228.

[5] R. Dickie, R. Cahill, H. S. Gamble, V. F. Fusco, A. Schuchinsky, and N. Grant, "Spatial demultiplexing in the sub-mm wave band using multilayer free-standing frequency selective surfaces," *IEEE Trans. Antennas Propag.*, vol. 53, no. 6, pp. 1903–1911, Jun. 2005.

[6] R. Dickie, R. Cahill, H. S. Gamble, V. F. Fusco, M. Henry, M. L. Oldfield, P. G. Huggard, P. Howard, N. Grant, Y. Munro, and P. de Maagt, "Submillimeter wave frequency selective surface with polarization independent spectral responses," *Proc. IEEE Antennas and Propagation*, vol. 57, pp. 1985–1994, Jul. 2009.

[7] R. Cahill, W. J. Hall, and R. J. Martin, "Technologies for millimeter remote sensing antennas," in *IEE/SEE Seminar Dig. on Spacecraft Antennas*, 1994, pp. 8/1–8/8.

[8] R. Cahill and E. A. Parker, "Frequency selective surface design for submillimetric demultiplexing," *Microw. Opt. Technol. Lett.*, vol. 7, pp. 595–597, Sep. 1994.

[9] R. Cahill, I. M. Sturland, J. W. Bowen, E. A. Parker, and A. C. de C Lima, "Frequency selective surfaces for millimetre and submillimetre wave quasi-optical demultiplexing," *Int., J. Infrared and Millimetre Waves*, vol. 14, pp. 1769–1788, Sept. 1993.

[10] R. Cahill and E. A. Parker, "Performance of mm-wave frequency selective surfaces in large incident angle quasi-optical systems," *Electron. Lett.*, vol. 28, pp. 788–789, Apr. 1992.

[11] R. Cahill, E. A. Parker, and I. M. Sturland, "Influence of substrate loss tangent on performance of multilayer sub millimetre wave FSS," *Electron. Lett.*, vol. 31, pp. 1752–1753, Sep. 1995.

[12] R. Cahill, H. S. Gamble, V. F. Fusco, J. C. Vardaxoglou, M. Jayawardene, B. Moyna, M. Oldfield, G. Cox, and N. Grant, "Low loss FSS for channel demultiplexing and image band rejection filtering," in *Proc 24th ESTEC AntennaWorkshop on Innovative Periodic Antennas: Photonic Bandgap, Fractal and Freq. Sel. Surfaces*, May 2001, pp. 103–108.

[13] B. A. Munk, *Frequency Selective Surfaces Theory and Design*. Hoboken, NJ: Wiley, 2000.

[14] R. Cahill, J. C. Vardaxaglou, and M. Jayawardene, "Two layer mm-wave FSS of linear slot elements with low insertion loss," *Proc. IEE Microw. Antennas and Propag.*, vol. 148, pp. 410–412, Dec. 2001.

[15] S. Biber, M. Bozzi, O. Gunther, L. Perregrini, and L. P. Schmidt, "Design and testing of frequency-selective surfaces on silicon substrates for submillimeter-wave applications," *IEEE Trans. Antennas Propag.*, vol. 1, no. 9, pp. 2638–2645, Sep. 2006, 54.

[16] R. Dickie, R. Cahill, V. F. Fusco, H. S. Gamble, B. Moyna, P. Huggard, N. Grant, and C. Philpot, "300 GHz high Q resonant slot frequency selective surface filter," *Proc. IET Microw. Antennas and Propag.*, vol. 151, pp. 31–36, Jan. 2004.

[17] P. H. Siegel and J. A. Lichtenberger, "A technique for fabricating free standing electrically thick metallic mesh and parallel wire grids for use as millimetre and submillimetre wavelength filters and polarizers," in *IEEE MTT-S Int. Microwave Symp. Dig.*, May 1990, pp. 1311–1314.

[18] D. W. Porterfield, J. L. Hesler, R. Densing, E. R. Mueller, T. W. Crowe, and R. M. Weikle, "Resonant metal-mesh bandpass filters for the infrared," *Appl. Opt.*, vol. 33, pp. 6046–6052, Sept. 1994.

[19] M. E. MacDonald, A. Alexanian, R. A. York, Z. Popovic, and E. N. Grossman, "Spectral transmittance of lossy printed resonant-grid terahertz bandpass filters," *Proc. IEEE Trans. Microw. Theory Techn.*, vol. 48, pp. 712–718, April 2000.

[20] Ansoft Corp., "HFSS 3D EM simulation software for RF, wireless, packaging and optoelectronic design," (Mar. 2011) [Online]. Available: http://www.ansoft.com

[21] AB Millimetre, Paris, France, "AB Millimetre," (Mar. 2011) [Online]. Available: http://www.abmillimetre.com

[22] P. F. Goldsmith, "Quasi-optical techniques offer advantages at millimeter frequencies," *Microw. Syst. News*, pp. 65–84, Dec. 1983.

[23] R. Dickie, R. Cahill, V. F. Fusco, H. S. Gamble, Y. Munro, and S. Rea, "Recent advances in submillimetre wave FSS technology for passive remote sensing instruments," in *Proc. 4rd Eur. Conf. on Antennas and Propagation (EuCAP)*, Barcelona, Spain, Apr. 2010.

[24] CST-Computer Simulation Technology, Darmstadt, Germany, "CST-Comp. Simulation Technology," 2005 [Online]. Available: http://www.cst.com

[25] R. Dickie, R. Cahill, H. S. Gamble, V. F. Fusco, P. G. Huggard, B. Moyna, M. Oldfield, N. Grant, and P. de Maagt, "Polarisation independent bandpass FSS," *Electron. Lett.*, vol. 43, pp. 1013–1015, Sep. 2007.

[26] M. Euler, V. F. Fusco, R. Cahill, and R. Dickie, "325 GHz single layer sub-millimeter wave FSS based split slot ring linear to circular polarization convertor," *IEEE Trans. Antennas Propag.*, vol. 58, no. 7, pp. 2457–2459, Jul. 2010.

[27] B. Y. Toh, R. Cahill, and V. F. Fusco, "Understanding and measuring circular polarization," *IEEE Trans. Edu.*, vol. 46, no. 3, pp. 313–319, Aug. 2003.

[28] M. Euler, V. F. Fusco, R. Cahill, and R. Dickie, "Comparison of FSS based linear to circular polarization converter geometries," *Proc. IET Microw. Antennas and Propag.*, vol. 4, pp. 1764–1772, Nov. 2010.

[29] R. Simms, R. Dickie, R. Cahill, N. Mitchell, H. S. Gamble, and V. F. Fusco, "Measurement of electromagnetic properties of liquid crystals at 300 GHz using a tunable FSS," presented at the 32nd ESA Workshop on Antennas for Space Applications, Noordwijk, the Netherlands, Oct. 2010.

[30] W. Hu, R. Dickie, R. Cahill, H. S. Gamble, M. Y. Ismail, V. F. Fusco, D. Linton, S. P. Rea, and N. Grant, "Liquid crystal tunable mm wave frequency selective surface," *IEEE Microw. Wireless Compon. Lett.*, vol. 17, no. 9, pp. 667–700, Sep. 2007.

Raymond Dickie received the B.Eng. (Hons) and Ph.D. degrees in electrical and electronic engineering from The Queen's University of Belfast, U.K., in 2001 and 2004, respectively.

In October 2004 he joined the high frequency electronic circuits and antennas group at The Institute of Electronics, Communications and Information Technology (ECIT), Belfast, U.K., where he is now employed as a senior engineer working on mm-wave components. His work on freestanding frequency selective surfaces has been patented and includes fabrication methods using silicon-on-insulator (SOI), metal and polymer mesh technology. He has experience in photolithographic processing including thick positive and negative photoresist RIE of polymers and oxides, DRIE of silicon, CVD metal deposition, high conductivity stress controlled electroplating, and SEM imaging methods. He is experienced in working in clean room environments where he develops MEMS devices. He has co authored over 50 publications, his high frequency research interests include numerical modeling of high frequency structures and precision quasi-optical measurements in the millimeter and sub-millimeter wave bands.

Robert Cahill (M'10–SM'11) received the B.Sc. (1st class, Hons) degree in physics from the University of Aston, Birmingham, U.K., in 1979, and the Ph.D. degree in microwave electronics from the University of Kent, Canterbury, U.K., in 1982.

He joined The Queen's University of Belfast (QUB), U.K., in 1999 after a 17–year career working in the UK space and defense industry, where he worked on antenna and passive microwave device technology projects. During this time he pioneered methods for predicting the performance of antennas on complex scattering surfaces such as satellites and has developed techniques for analyzing and fabricating mm and sub-mm wave quasi-optical dichroic filters. Recently, he has established a 100–700 GHz quasi-optical S-parameter measurement facility at QUB. He has exploited the results of numerous research projects, sponsored by the European Space Agency, EADS Astrium Space Ltd., the British National Space Agency, the Centre for Earth Observation Instrumentation (CEOI), and the UK Meteorological Office, to develop quasi-optical demultiplexers for atmospheric sounding radiometers in the range 89–500 GHz. These include AMSU-B, AMAS, MARSCHALS and the ESA 500 GHz demonstrator. His recent interests also include the characterization of liquid crystal materials at microwave and mm wavelengths, and strategies for broad banding and creating active reflectarray antennas. He has (co)—authored over 130 publications and holds four international patents.

Vincent Fusco (S'82–M'82–SM'96–F'04) received the Bachelors degree (1st class honors) in electrical and electronic engineering, the Ph_D. degree in microwave electronics, and the D.Sc. degree for his work on advanced front end architectures with enhanced functionality, from The Queens University of Belfast (QUB), Belfast, Northern Ireland, in 1979, 1982, and 2000, respectively.

He is the Technical Director of the High Frequency Laboratories at The Queens University of Belfast, U.K., and is also Director of the International Centre for Research for System on Chip and Advanced MicroWireless Integration, SoCaM. His research interests include nonlinear microwave circuit design, and active and passive antenna techniques. He has published over 420 scientific papers in major journals and international conferences, and is the author of two text books. He holds several patents on active and retrodirective antennas and has contributed invited chapters to books in the fields of active antenna design and EM field computation.

Dr. Fusco is a Fellow of the Royal Academy of Engineering, and a Fellow of the Institution of Electrical Engineers (U.K.). In 1986, he was awarded a British Telecommunications Fellowship, and in 1997 he was awarded the NI Engineering Federation Trophy for outstanding industrially relevant research.

Harold S. Gamble graduated from The Queen's University of Belfast with a 1st class honours degree in electrical and electronic engineering in 1966, and received the Ph.D. degree in 1969.

As a research engineer at The Standard Telecommunication Laboratories, Harlow, U.K., he established a polysilicon gate process for MOS integrated circuits. He was appointed to a lectureship at The Queen's University of Belfast, U.K., in 1973, and has lead research there in silicon device design and related technology including, CCDs, silicided shallow junctions, rapid thermal CVD, GTOs and Static Induction Thyristors. In 1992 he was promoted to Professor of Microelectronic Engineering, and until 2010 was the Director of the Northern Ireland Semiconductor Research Centre. Major activity at present is the use of direct silicon wafer bonding for producing silicon-on-insulator (SOI) substrates for low power bipolar transistor circuits. This includes trench and refill before bond technology and buried metallic layers to eliminate epitaxial layers and to minimize collector resistance. Ground plane SOI structures incorporating tungsten silicide layers are being investigated for cross talk suppression in mixed signal circuits and for ultra short MOSTs. The silicon wafer bonding combined with the integrated circuit patterning techniques is also being applied to micro-machining applications such as sensors, mechanical actuators and 3-D mm wave components. His other projects include multilayer free-standing frequency selective surfaces for spatial demultiplexing in the sub-mm wave band, thin film transistors in polysilicon or bonded silicon on glass for displays/imagers, and high density interconnects produced by sputtering and CVD for IC's and MR heads. He has co-authored over 250 publications in the area of silicon devices and thin film technology.

Neil Mitchell (M'96–SM'02) received the B.Sc. and Ph.D. degrees in electrical and electronic engineering from The Queen's University of Belfast, U.K., in 1982 and 1986, respectively.

In 1986 he was appointed as a temporary lecturer in Queen's University Belfast, U.K., where he is currently a senior lecturer in the School of Electronics, Electrical Engineering and Computer Science. His main research interests are in semiconductor and microelectromechanical systems technology. His research has encompassed a wide range of device structures and has included development of technology for fabrication of semiconductor devices on substrates including glass and sapphire. His recent research has been on technology for fabrication of germanium and germanium on sapphire devices. In the micromachining area, he has developed technology for fabrication of RF MEMS components and sensors for biomedical and environmental applications. Recent micromachining activity has been on chemotaxis sensors for biomedical applications, photoacoustic sensors for greenhouse gas measurement and frequency selective surfaces for RF applications. He is joint author of over 130 publications.